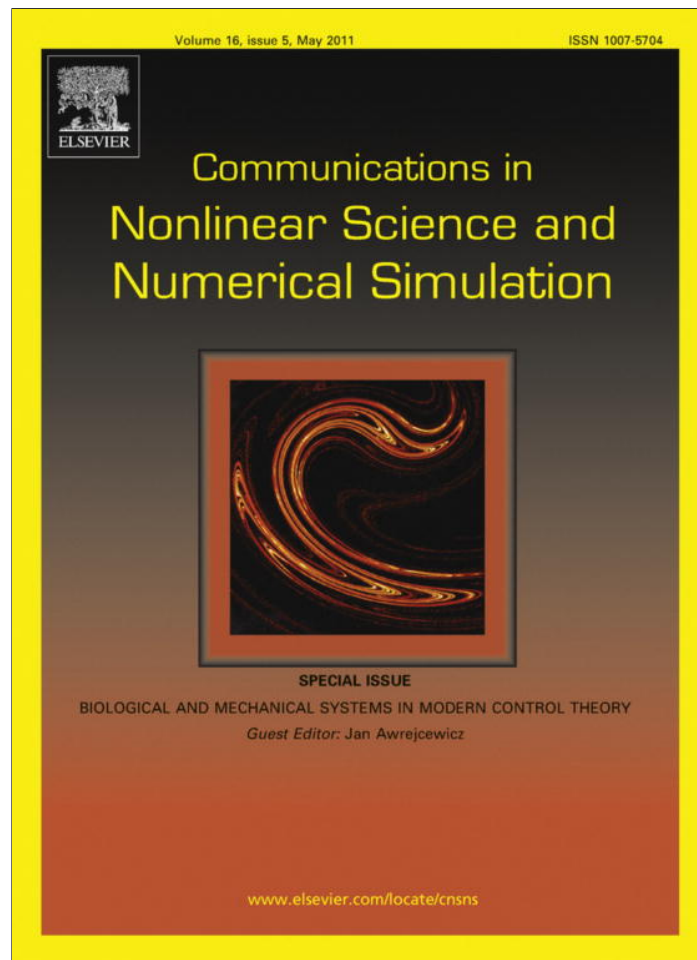


Provided for non-commercial research and education use.
Not for reproduction, distribution or commercial use.



This article appeared in a journal published by Elsevier. The attached copy is furnished to the author for internal non-commercial research and education use, including for instruction at the authors institution and sharing with colleagues.

Other uses, including reproduction and distribution, or selling or licensing copies, or posting to personal, institutional or third party websites are prohibited.

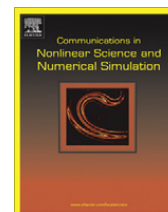
In most cases authors are permitted to post their version of the article (e.g. in Word or Tex form) to their personal website or institutional repository. Authors requiring further information regarding Elsevier's archiving and manuscript policies are encouraged to visit:

<http://www.elsevier.com/copyright>



Contents lists available at ScienceDirect

Commun Nonlinear Sci Numer Simulat

journal homepage: www.elsevier.com/locate/cnsns

Computed torque control of an under-actuated service robot platform modeled by natural coordinates

Ambrus Zelei^{a,*}, László L. Kovács^b, Gábor Stépán^a^a Department of Applied Mechanics, Budapest University of Technology and Economics, H-1521 Budapest, P.O. Box. 91, Hungary^b HAS-BME Research Group on Dynamics of Machines and Vehicles, H-1521 Budapest, P.O. Box. 91, Hungary

ARTICLE INFO

Article history:

Available online 8 July 2010

Keywords:

Computed torque control
Under-actuated systems
Crane systems
Differential–algebraic equations

ABSTRACT

The paper investigates the motion planning of a suspended service robot platform equipped with ducted fan actuators. The platform consists of an RRT robot and a cable suspended swinging actuator that form a subsequent parallel kinematic chain and it is equipped with ducted fan actuators. In spite of the complementary ducted fan actuators, the system is under-actuated. The method of computed torques is applied to control the motion of the robot.

The under-actuated systems have less control inputs than degrees of freedom. We assume that the investigated under-actuated system has desired outputs of the same number as inputs. In spite of the fact that the inverse dynamical calculation leads to the solution of a system of differential–algebraic equations (DAE), the desired control inputs can be determined uniquely by the method of computed torques.

We use natural (Cartesian) coordinates to describe the configuration of the robot, while a set of algebraic equations represents the geometric constraints. In this modeling approach the mathematical model of the dynamical system itself is also a DAE.

The paper discusses the inverse dynamics problem of the complex hybrid robotic system. The results include the desired actuator forces as well as the nominal coordinates corresponding to the desired motion of the carried payload. The method of computed torque control with a PD controller is applied to under-actuated systems described by natural coordinates, while the inverse dynamics is solved via the backward Euler discretization of the DAE system for which a general formalism is proposed. The results are compared with the closed form results obtained by simplified models of the system. Numerical simulation and experiments demonstrate the applicability of the presented concepts.

© 2010 Elsevier B.V. All rights reserved.

1. Introduction

Obstacle avoidance is an important problem in service and mobile robotics, especially when the robots have to move in an everyday indoor environment. Static obstacles on the floor of a room include various objects such as stairs, doorsteps, chairs, tables and even the edge of carpets. In addition, floor based domestic robots need to have strategies to overcome randomly placed objects, e.g., children toys left on the floor. Hence, these robots need improved sensing capabilities and control, or the use of auxiliary devices, e.g., virtual walls to avoid obstacles.

A new direction in the development of indoor service robots is the use of robotic structures that can move on the almost obstacle free ceiling of a room, while transport the payload or an actuator mechanism similarly to gantry cranes. For

* Corresponding author.

E-mail addresses: zelei.ambrus@gmail.com (A. Zelei), kovacs@mm.bme.hu (L.L. Kovács), stepan@mm.bme.hu (G. Stépán).

example, the Flora ceiling absorbed service robot [9] utilizes permanent magnets to keep and move its mobile cart on the ceiling, and its working unit is actuated by three telescopic arms in the vertical direction.

A design of a tethered aerial robot is presented by McKerrow and Ratner [10], in which the working unit is suspended on a single cable and equipped with two ducted fan actuators. The system is transported by an unmanned aerial vehicle, and the fans are used to stabilize the motion of the working unit that carries tiny robotic agents, which are used for exploring tasks in rescue operations. Although the described service robotic application is outdoor by itself, the concept can be realized in indoor environments by substituting the aerial vehicle with a ceiling based transporting unit.

The above solutions solve the problem of avoiding obstacles on the floor, while they are able to roam over almost the whole inner space of a room, and compared to gantry cranes, they enable the use of co-operating multiple units. Cable suspended structures provide larger vertical workspace and they are lightweight, however, the limited possibility of the actuation of the suspended payload is a critical issue.

The present paper describes a new indoor service robot locomotion technology developed within the ACROBOTER (IST-2006-045530) project [7]. The suspended payload platform is equipped with windable complementary orienting cables and ducted fan actuators in order to make the payload position and orientation controllable.

Cranes are pendulum-like structures that are widely used for transporting a payload to a specified position which is usually accurately defined. Additionally, the payload sometimes has to follow a prescribed spatial trajectory, too. Since cranes are nonlinear oscillating systems, it is a complicated task to achieve a good motion control which suppresses the swinging motion of the payload. In the case of general cranes such as tower cranes, gantry cranes or overhead cranes the position control of the payload is realized by the controlled movement of the top mounting point of the cable. The low actuating possibilities also complicate the controlling strategies. The oscillating behavior of floating and aerial cranes significantly becomes more intense because the position of the top mounting point is disturbed by environmental effects such as waves and wind.

In order to achieve high efficiency, the automation of the crane movements is significant. Several controlling strategies have been developed; most commonly feedback controllers [13] and time delayed feedback controllers are used for oscillation suppression [5,13]. In order to attain better anti-sway control fuzzy logic controllers [13] are also used.

Cranes and the ACROBOTER robot are under-actuated systems, because they have lower number of control inputs than degrees of freedom (DoFs). The following mathematical definition of under-actuated mechanical systems is adapted from [1,2]. The generalized mathematical model of the dynamical system can be written as:

$$\ddot{\mathbf{q}} = \mathbf{f}(\mathbf{q}, \dot{\mathbf{q}}) + \mathbf{G}(\mathbf{q})\mathbf{u}, \quad (1)$$

where \mathbf{q} is a vector of independent generalized coordinates, \mathbf{f} is a vector field that determines the dynamics of the system, \mathbf{G} the input matrix, and \mathbf{u} is the vector of generalized inputs. The system is under-actuated if the rank of \mathbf{G} is smaller than the dimension of \mathbf{q} . Thus, if a dynamical system contains less independent actuators than the degrees of freedom it has, the system is under-actuated.

2. The ACROBOTER platform

Structure and the first prototype of the ACROBOTER service robotic platform [7,12] are presented in Fig. 1. The system is attached to the ceiling by using anchor points that are simple and passive elements providing fixation and through which the

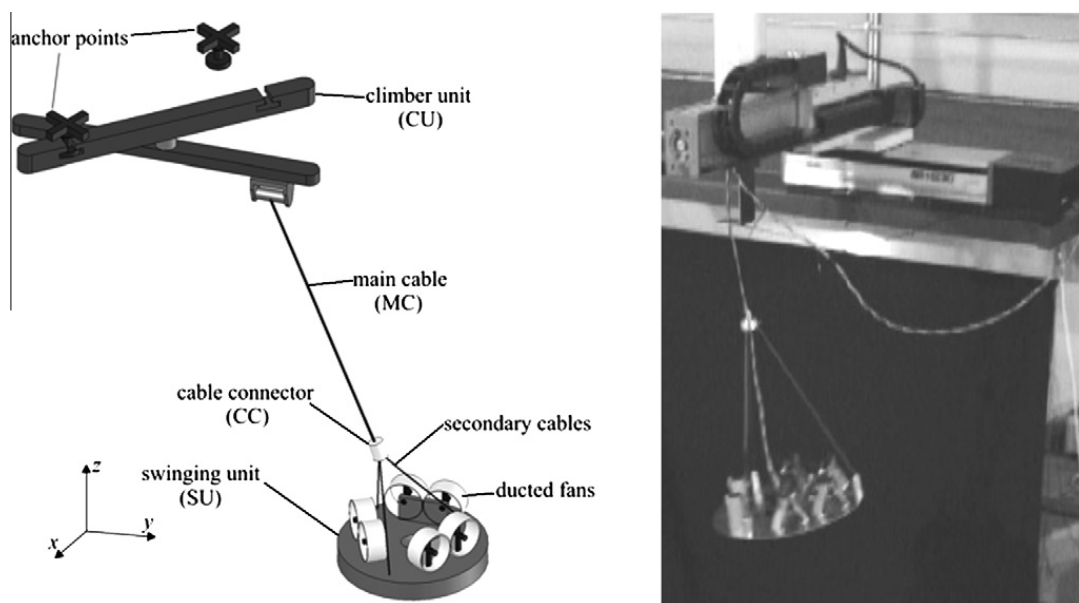


Fig. 1. Structure (left) and the first prototype (right) of the ACROBOTER platform.

power is supplied. The climber unit (CU) is an RRT robot which can move in a grid of anchor points and transport the working unit of the system in the horizontal direction. The used planar RRT structure is redundant and provides smooth change of anchor points with respect to the motion of its end-effector, i.e., the winding actuator of the main suspending cable (MC). The lower end of the main suspending cable is attached to the cable connector (CC), which clamps three additional windable cables that orient the base plate of the swinging unit (SU). The swinging unit is equipped with six ducted fan actuators which generate thrust forces parallel to the plane of the base plate and a torque that can rotate the swinging unit at the same time. A mechanical interface is attached to the bottom of the swinging unit that serves as a tool changer with electrical connections.

From the point of view of dynamics modeling, the small sized cable connector can be considered as point mass and the weight of the cables can be neglected. Then the degrees of freedom (DoFs) of the whole system is 12 in total containing the 3 plus 3 DoFs of the climber unit and the cable connector, and the 6 DoFs of the swinging unit, respectively. The actuators of the system is the three joint drives of the climber unit, the four cable winches and the effective thrust forces (a coplanar and perpendicular pair) and torque provided by the ducted fans. Consequently, despite of these complementary actuators, the system is still under-actuated. This analysis refers to the fact that the cable connector can only be actuated by the windable cables and its horizontal position cannot directly be actuated. Moreover, the vertical position of the swinging unit is determined by both the lengths of the secondary cables and the main cables, which makes the system kinematically redundant.

3. Method of computed torques

3.1. Introduction

In this work we assume that the system has desired outputs of the same number as control inputs [6,12]. The servo constraints define the desired system outputs accordingly to the task [6,11]. In spite of the fact that the inverse dynamical calculation leads to the solution of a system of differential algebraic equations (DAE), the desired control inputs can be determined uniquely by the computed torque method generalized for under-actuated systems.

Several dynamical systems, especially robots with parallel kinematic chains have a complex dynamics, which may hardly be modeled using conventional robotic approaches. An alternative modeling technique is to use natural (Cartesian) coordinates to describe the configuration of the robot. The number of descriptor coordinates is larger than the DoFs thus a set of algebraic equations represents the geometric constraints. In this approach the dynamics of the controlled system is modeled by a DAE.

The generalization of computed torque control for under-actuated systems is discussed in [14]. The method called CDCTC (computed desired computed torque control) can be applied only for systems that are represented by minimum number generalized coordinates $\bar{\mathbf{q}}$, and the mathematical model is an ODEs:

$$\mathbf{M}(\bar{\mathbf{q}})\ddot{\bar{\mathbf{q}}} + \mathbf{f}(\bar{\mathbf{q}}, \dot{\bar{\mathbf{q}}}, t) = \mathbf{H}(\bar{\mathbf{q}})\mathbf{u}, \quad (2)$$

where \mathbf{M} is the mass matrix, $\mathbf{f}(\bar{\mathbf{q}}, \dot{\bar{\mathbf{q}}}, t)$ represents the external and internal forces except the control forces, \mathbf{H} is the input matrix and \mathbf{u} is the input vector. The phrase “computed desired” means that the uncontrolled coordinates cannot be arbitrarily prescribed but they can be calculated from the internal dynamics of the controlled system. Contrarily the controlled coordinates are prescribed. The control law that eliminates the error of the controlled coordinates at $t \rightarrow \infty$ is:

$$\mathbf{H}(\bar{\mathbf{q}}^d)\mathbf{u} = \mathbf{M}(\bar{\mathbf{q}}^d)\ddot{\bar{\mathbf{q}}}^d + \mathbf{f}(\bar{\mathbf{q}}^d, \dot{\bar{\mathbf{q}}}^d, t) + \mathbf{K}_p(\bar{\mathbf{q}}^d - \bar{\mathbf{q}}) + \mathbf{K}_D(\dot{\bar{\mathbf{q}}}^d - \dot{\bar{\mathbf{q}}}), \quad (3)$$

where \mathbf{K}_p and \mathbf{K}_D are the gain matrices of the linear compensator. Eq. (3) has to be solved for the control input \mathbf{u} and for the uncontrolled subset of generalized coordinates $\bar{\mathbf{q}}$. The basic idea is to use the null space \mathbf{N} of the input matrix \mathbf{H} to project the equations into the space of the uncontrolled motion (4). The projected system can be solved for the uncontrolled coordinates. If we know the uncontrolled coordinates, the control inputs can be determined by Eq. (5)

$$\mathbf{0} = \mathbf{N}^T [\mathbf{M}(\bar{\mathbf{q}}^d)\ddot{\bar{\mathbf{q}}}^d + \mathbf{f}(\bar{\mathbf{q}}^d, \dot{\bar{\mathbf{q}}}^d, t) + \mathbf{K}_p(\bar{\mathbf{q}}^d - \bar{\mathbf{q}}) + \mathbf{K}_D(\dot{\bar{\mathbf{q}}}^d - \dot{\bar{\mathbf{q}}})], \quad (4)$$

$$\mathbf{u} = (\mathbf{H}(\bar{\mathbf{q}}^d)^T \mathbf{H}(\bar{\mathbf{q}}^d))^{-1} \mathbf{H}(\bar{\mathbf{q}}^d)^T [\mathbf{M}(\bar{\mathbf{q}}^d)\ddot{\bar{\mathbf{q}}}^d + \mathbf{f}(\bar{\mathbf{q}}^d, \dot{\bar{\mathbf{q}}}^d, t) + \mathbf{K}_p(\bar{\mathbf{q}}^d - \bar{\mathbf{q}}) + \mathbf{K}_D(\dot{\bar{\mathbf{q}}}^d - \dot{\bar{\mathbf{q}}})]. \quad (5)$$

It is possible to adopt the CDCTC method for natural coordinate based system, which is described by a redundant set of descriptor coordinates \mathbf{q} and the equations of motion constitute a DAE. The solution requires an additional projection [8] that results an ODE. After the projection the CDCTC method can be applied, but it may be computationally too expensive because of the repeated projections.

Instead of the application of the CDCTC method we solve the inverse dynamic problem via the backward Euler discretization of the DAE system. The backward method requires the solution of a system of nonlinear algebraic equations in each time step, which is solved by Newton–Raphson iteration. A general formalism is proposed for the analytical calculation of the Jacobian of the Newton–Raphson method.

The results are presented in the form of a case study for the ACROBOTER system and confirmed by numerical simulation. The numerical results are compared with analytical calculations.

3.2. Problem formulation

By using the redundant set of descriptor coordinates \mathbf{q} the equation of motion, the geometric constraint vector of the system and the servo constraint vector can be written as:

$$\mathbf{M}\ddot{\mathbf{q}} + \Phi_{\mathbf{q}}^T(\mathbf{q})\lambda = \mathbf{Q}_g + \mathbf{H}(\mathbf{q})\mathbf{u}, \tag{6}$$

$$\boldsymbol{\varphi}(\mathbf{q}) = \mathbf{0}, \tag{7}$$

$$\boldsymbol{\varphi}_s(\mathbf{q}, \mathbf{p}(t)) = \mathbf{0}. \tag{8}$$

Eq. (6) is the Lagrangian equation of motion of the first kind, where \mathbf{M} is the $n \times n$ sized constant matrix [3]. Symbol \mathbf{Q}_g is the generalized gravity force. The m number of geometric constraints are represented by the vector $\boldsymbol{\varphi}(\mathbf{q})$ in (7) and $\Phi_{\mathbf{q}}(\mathbf{q})$ is the Jacobian matrix of the constraints. The corresponding Lagrange multipliers are denoted by λ . The l dimension input vector is \mathbf{u} and the $n \times l$ sized $\mathbf{H}(\mathbf{q})$ is the generalized input matrix.

The number l of the control inputs is less than the $n - m$ DoFs of the system, thus it is under-actuated. The task of the robot is formulated by the servo constraint vector $\boldsymbol{\varphi}_s(\mathbf{q}, \mathbf{p}(t))$ [6,11] given in Eq. (8). The dimension of the servo constraint vector is also l that means the l number of control inputs can uniquely be determined.

The servo constraints depend on the function $\mathbf{p}(t)$ that can be handled as the desired system output and it may describe the desired trajectory of a certain point and/or the desired orientation of the end-effector. The servo constraints can be formulated as:

$$\boldsymbol{\varphi}_s(\mathbf{q}, \mathbf{p}(t)) = \mathbf{h}(\mathbf{q}) - \mathbf{p}(t), \tag{9}$$

where $\mathbf{h}(\mathbf{q})$ gives the prescribed system outputs as the function of the descriptor coordinates. We assume that the servo constraints and a well chosen subset of geometric constraints can be solved for the controlled coordinates \mathbf{q}_c in closed form. Then the task can be defined by $\mathbf{q}_c = \mathbf{q}_c^d$, where the superscript d refers to the desired value. Important to notice that the computed torque control method by direct discretization does not require to use $\mathbf{q}_c = \mathbf{q}_c^d$, because the direct discretization can handle the full constraint system composed by $\boldsymbol{\varphi}(\mathbf{q})$ and $\boldsymbol{\varphi}_s(\mathbf{q}, \mathbf{p}(t))$, but the size of the system increases.

For the partitioning of the descriptor coordinates we introduce the vector of controlled coordinates with $\mathbf{q}_c = \mathbf{S}_c^T \mathbf{q}$ and $\mathbf{q}_u = \mathbf{S}_u^T \mathbf{q}$, respectively [14], where \mathbf{S}_c and \mathbf{S}_u are task dependent selector matrices. The vector of descriptor coordinates can be reassembled as $\mathbf{q} = \mathbf{S}_c \mathbf{q}_c + \mathbf{S}_u \mathbf{q}_u$.

Summarizing, the aim is to determine the desired value of the uncontrolled coordinates \mathbf{q}_u , the input vector \mathbf{u} and adjuntively the Lagrange multipliers λ that satisfies the differential algebraic equation system (6)–(8). In some simplified cases this calculation can be done analytically. Section 4 presents analytical results for the simplified models of the ACROBOTER platform.

4. Analytical inverse dynamics

In case of under-actuated systems the solution of the inverse kinematics problem naturally involves dynamic calculations. In addition, the redundancy of ACROBOTER may be resolved by optimization. However, applying some reasonable simplifications the complex problem of the inverse dynamical calculation of the under-actuated and redundant robot can be converted into the inverse dynamical problem of a double pendulum system. For brevity the method is presented for the spatial double pendulum, but the results are compared with the planar model of ACROBOTER only. The investigated pendulum models and the complete planar model are presented in Fig. 2.

4.1. Single pendulum model

The ducted fan actuators generate typically low thrusts compared to the possible total weight of the robot including the payload. Thus they can be excluded from the dynamical model during inverse dynamical calculation and they are only employed to eliminate the small disturbances. The prescribed trajectories of the climber unit and the windable cables have to be determined to provide the desired pendulum-like motion of the platform during which the orientation of the swinging unit is kept constant (e.g., horizontal) by the secondary cables (see Fig. 1). In the control of the system this trajectory can be used for calculating feedforward torques for the corresponding actuators, while the ducted fans can be used for stabilizing the motion of the swinging unit along its prescribed trajectory. In addition, since the cable connector has much lower weight than the swinging unit, the cable connector might be seen as a source of high frequency but small disturbances, only.

These considerations lead to the single pendulum model presented on the left in Fig. 2, where the point mass, m_{SU} stands for the swinging unit. The inputs of the inverse calculation are the desired positions x^d, y^d and z^d of the center of mass of the swinging unit.

The goal of the inverse dynamics tasks is to define the corresponding desired trajectory of the climber unit denoted by x_{CU}^d and y_{CU}^d , the desired forces which formulates the control input vector: $\mathbf{u} = [F_x^d, F_y^d, F_c^d]^T$, and the nominal cable length l^d in closed form. Forces F_x and F_y are the forces that acts on the top mounting point of the cable and F_c is the cable force. The matrix equation of motion of the single pendulum model can be expressed with descriptor coordinates $q = [x_{CU}, y_{CU}, x, y, z]^T$ in the form:

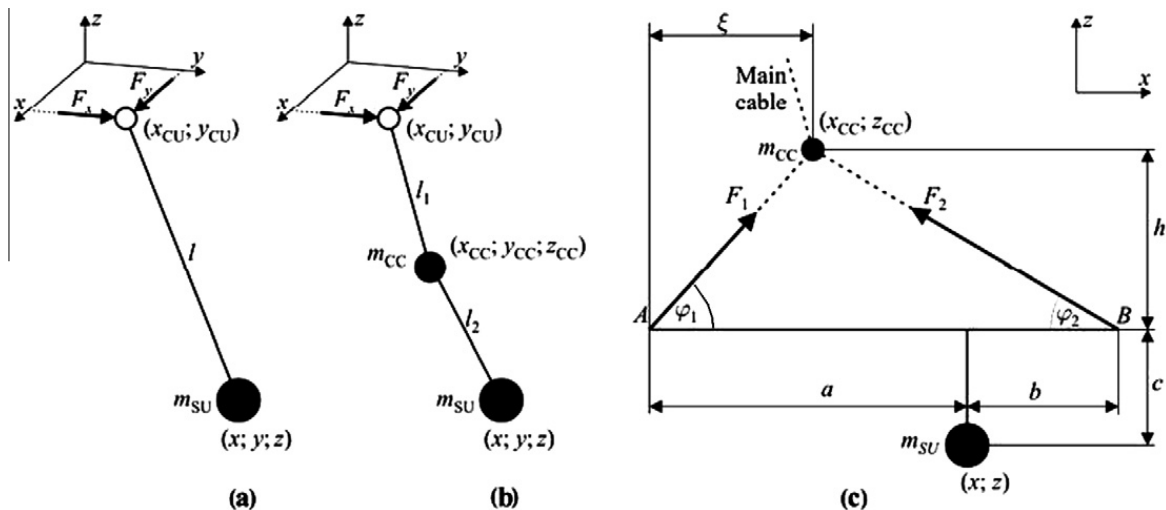


Fig. 2. Single pendulum (left), double pendulum (middle) and complete planar models (right).

$$\begin{bmatrix} 0 & 0 & 0 & 0 & 0 \\ 0 & 0 & 0 & 0 & 0 \\ 0 & 0 & m_{SU} & 0 & 0 \\ 0 & 0 & 0 & m_{SU} & 0 \\ 0 & 0 & 0 & 0 & m_{SU} \end{bmatrix} \begin{bmatrix} \ddot{x}_{CU} \\ \ddot{y}_{CU} \\ \ddot{x} \\ \ddot{y} \\ \ddot{z} \end{bmatrix} + \begin{bmatrix} 0 \\ 0 \\ 0 \\ 0 \\ m_{SU}g \end{bmatrix} = \begin{bmatrix} F_x + F_c(x - x_{CU})/l \\ F_y + F_c(y - y_{CU})/l \\ -F_c(x - x_{CU})/l \\ -F_c(y - y_{CU})/l \\ -F_c z/l \end{bmatrix}, \quad (10)$$

where the cable length is expressed as

$$l = \sqrt{(x_{CU} - x)^2 + (y_{CU} - y)^2 + z^2}. \quad (11)$$

The task is defined by the servo constraint vector with $\mathbf{h}(\mathbf{q}) = [x, y, z]^t$ and $\mathbf{p}(t) = [x^d(t), y^d(t), z^d(t)]^T$. The dimension of the servo constraint vector is three since the number of control inputs is also three. The servo constraint can be formulated as:

$$\Phi_s(\mathbf{q}, \mathbf{p}(t)) = [x - x^d, y - y^d, z - z^d]^T. \quad (12)$$

The servo constraints can easily be solved for the desired value of the controlled coordinates $x = x^d, y = y^d$ and $z = z^d$. From the equations of motion we can calculate the desired or in other words the nominal values of the uncontrolled coordinates x_{CU}^d and y_{CU}^d which gives the desired trajectory of the climber unit and the control forces F_x^d, F_y^d and F_c^d as follows:

$$x_{CU}^d = x^d - \frac{\ddot{x}^d z^d}{\ddot{z}^d + g}, \quad (13)$$

$$y_{CU}^d = y^d - \frac{\ddot{y}^d z^d}{\ddot{z}^d + g}, \quad (14)$$

$$F_x^d = m_{SU} \ddot{x}^d, \quad (15)$$

$$F_y^d = m_{SU} \ddot{y}^d, \quad (16)$$

$$F_c^d = -m_{SU} l^d \frac{\ddot{z}^d + g}{z^d}. \quad (17)$$

With the above formulae (13)–(17) it is straightforward to calculate the desired length of the main suspending cable from Eq. (11), and the corresponding winding torque can also be expressed by knowing the dynamics of the winding actuator.

An important result of the above calculation is that the use of the single pendulum model in trajectory generation of the climber unit requires C^4 continuity of the desired swinging unit trajectory.

This is because the climber unit trajectories need to be two times continuously differentiable to have smooth desired accelerations.

4.2. Double pendulum model

A further step in modeling the ACROBOTER platform could be the double pendulum model presented in the middle of Fig. 2. Beyond enabling a more accurate calculation of the desired trajectory of the climber unit this model makes it possible to consider the redundant actuation of the windable cables in the vertical direction. In the following the vertical distance

$z_{CC} - z$ between the swinging unit and the cable connector (see middle of Fig. 2) is considered as a desired parameter that can be obtained as a fixed value by experiments or it can be calculated based on some optimization method.

In the case of the double pendulum model the control input vector contains the lateral forces acting on the top mounting point of the upper pendulum and the two cable forces that acts on the cable lengths l_1 and l_2 . Thus the control input is $\mathbf{u} = [F_x^d, F_y^d, F_{C1}^d, F_{C2}^d]$. The equation of motion is written with the coordinates $\mathbf{q} = [x_{CU}, y_{CU}, x_{CC}, y_{CC}, z_{CC}, x, y, z]^T$ in the following matrix form:

$$\begin{bmatrix} 0 \\ 0 \\ m_{CC}\ddot{x}_{CC} \\ m_{CC}\ddot{y}_{CC} \\ m_{CC}\ddot{z}_{CC} \\ m_{SU}\ddot{x} \\ m_{SU}\ddot{y} \\ m_{SU}\ddot{z} \end{bmatrix} + \begin{bmatrix} 0 \\ 0 \\ 0 \\ 0 \\ m_{CC}g \\ 0 \\ 0 \\ m_{SU}g \end{bmatrix} = \begin{bmatrix} F_x + F_{C1}(x_{CC} - x_{CU})/l_1 \\ F_y + F_{C1}(y_{CC} - y_{CU})/l_1 \\ -F_{C1}(x_{CC} - x_{CU})/l_1 + F_{C2}(x - x_{CC})/l_2 \\ -F_{C1}(y_{CC} - y_{CU})/l_1 + F_{C2}(y - y_{CC})/l_2 \\ -F_{C1}z_{CC}/l_1 + F_{C2}(z - z_{CC})/l_2 \\ -F_{C2}(x - x_{CC})/l_2 \\ -F_{C2}(y - y_{CC})/l_2 \\ -F_{C2}(z - z_{CC})/l_2 \end{bmatrix}. \tag{18}$$

Besides the desired motion of the system is defined by the four dimensional servo constraint with $\mathbf{p}(t) = [x^d(t), y^d(t), z^d(t), h_{CC}^d(t)]^T$, where $h_{CC}^d(t)$ is the desired elevation of the cable connector above the swinging unit and with $\mathbf{h}(\mathbf{q}) = [x, y, z, z_{CC} - z]^T$:

$$\boldsymbol{\varphi}_s(\mathbf{q}, \mathbf{p}(t)) = [x - x^d, y - y^d, z - z^d, z_{CC} - z - h_{CC}^d]^T. \tag{19}$$

Afterwards the inverse kinematics and dynamics of the double pendulum model can be solved in two steps. First the swinging unit can be considered as a single pendulum attached to the cable connector which is interpreted as a floating suspension point above the swinging unit at a desired elevation. Then the resulting trajectory of the cable connector plays the role of the desired trajectory of the bob of a single pendulum system composed of the cable connector and the climber unit. Consequently, the desired trajectories of the cable connector can be expressed similar to Eqs. (13), and (14) in the form

$$x_{CC}^d = x^d + \frac{\ddot{x}^d h_{CC}^d}{\ddot{z}^d + g}, \tag{20}$$

$$y_{CC}^d = y^d + \frac{\ddot{y}^d h_{CC}^d}{\ddot{z}^d + g}, \tag{21}$$

$$z_{CC}^d = z^d + h_{CC}^d. \tag{22}$$

The desired motion of the swinging unit is provided by the force delivered through its suspending cable:

$$F_{C2}^d = \frac{m_{SU}l_2(\ddot{z}^d + g)}{h_{CC}^d}. \tag{23}$$

As a second step the desired trajectory of the climber unit can be calculated as:

$$x_{CU}^d = x_{CC}^d + \frac{F_{C2}^d(x^d - x_{CC}^d) - m_{CC}l_2\ddot{x}_{CC}^d}{m_{CC}l_2(\ddot{z}^d + \ddot{h}_{CC}^d + g) - F_{C2}^d h_{CC}^d} (h_{CC}^d + z^d), \tag{24}$$

$$y_{CU}^d = y_{CC}^d + \frac{F_{C2}^d(y^d - y_{CC}^d) - m_{CC}l_2\ddot{y}_{CC}^d}{m_{CC}l_2(\ddot{z}^d + \ddot{h}_{CC}^d + g) - F_{C2}^d h_{CC}^d} (h_{CC}^d + z^d). \tag{25}$$

Finally the cable force in the upper pendulum which stands for the main cable force:

$$F_{C1}^d = -l_1 \frac{m_{CC}l_2(\ddot{z}_{CC}^d + \ddot{h}_{CC}^d + g) + F_{C2}^d h_{CC}^d}{l_2(z^d + h_{CC}^d)}. \tag{26}$$

A numerical example can be seen in Fig. 3. The desired x trajectory of the swinging unit is given by a six degree polynomial function, while the desired y trajectory is $y^d = 0$ and the desired vertical trajectory is given by the desired values $z^d = -1.5$ m and $h_{CC}^d = 0.35$ m.

Fig. 3 shows that a significant difference shows up between the desired x_{CU} trajectory calculated by the single or by the double pendulum model.

4.3. Complete planar model

In order to present the applicability of the results obtained for the single and double pendulum models, the complete planar model of ACROBOTER (see right in Fig. 2) is considered which also includes the secondary (orienting) cables of the swinging unit.

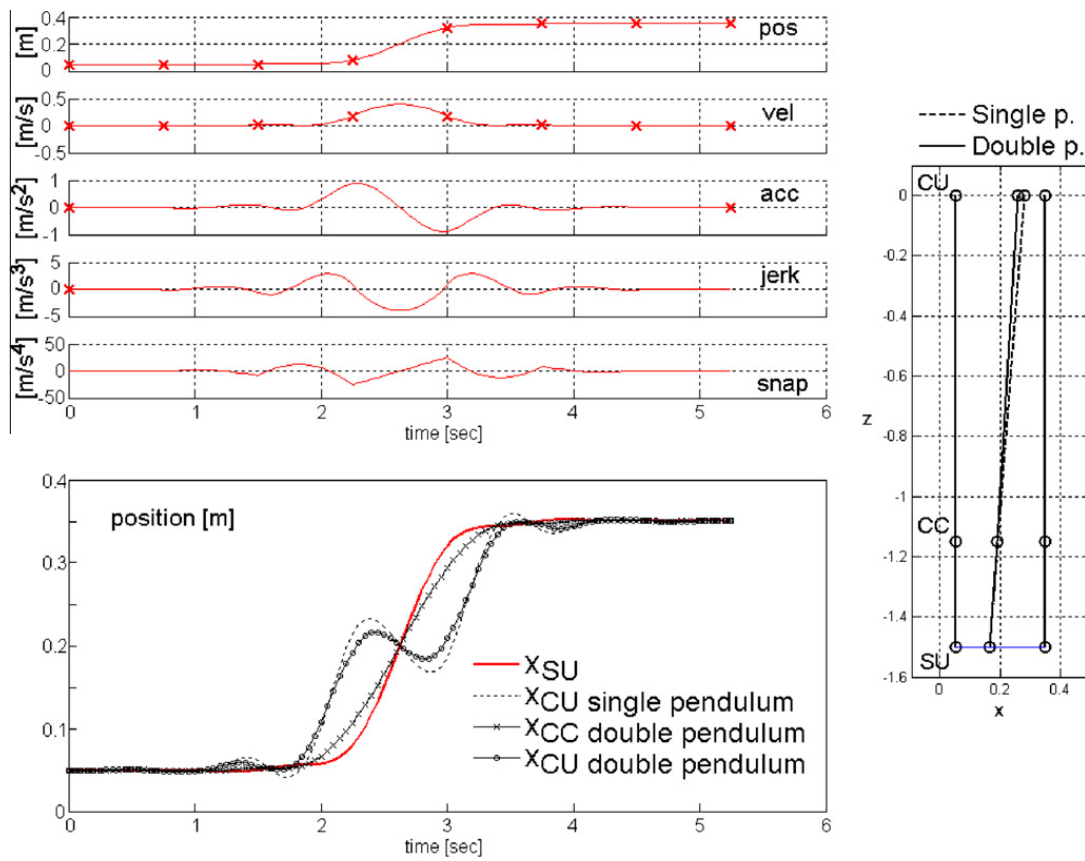


Fig. 3. Numerical example for the inverse calculation of the single pendulum and the double pendulum model.

The dimension of the swinging unit is characterized by the variables a and b , which together with the vertical distance c describes the location of the center of mass of the unit. In addition, coordinate ξ denotes the relative distance of the cable connector to the rod that represent the swinging unit, while h is the elevation of the cable connector above the swinging unit.

The desired orientation of the swinging unit is considered to be fixed, and without the loss of generality it is assumed that the swinging unit is kept always horizontal by the secondary orienting cables. This restriction is reasonable in a wide range of possible applications, such as pick and place objects in indoor environments.

The desired horizontal orientation of the swinging unit implies that the corresponding angular acceleration is zero, which yields the equation of motion of the planar model in the simplified form

$$m\ddot{x} = F_1 \cos \varphi_1 - F_2 \cos \varphi_2, \tag{27}$$

$$m\ddot{z} = F_1 \sin \varphi_1 + F_2 \sin \varphi_2 - mg \text{ and} \tag{28}$$

$$0 = -F_1(a \sin \varphi_1 + c \cos \varphi_1) + F_2(b \sin \varphi_2 + c \cos \varphi_2), \tag{29}$$

where F_1 and F_2 are the cable forces of the orienting cables and φ_1 and φ_2 are their angles at the swinging unit, respectively.

In Eqs. (27)–(29) the number of unknown parameters is 5 in total: ξ, F_1, F_2, φ_1 and φ_2 , since the trajectories $x(t)$ and $y(t)$ of the center of mass of the swinging unit are prescribed. When the elevation h of the cable connector above the swinging unit is also a desired parameter, the necessary independent constraint equations can be formulated for the cable angles as:

$$\cos \varphi_1 = \frac{\xi}{\sqrt{\xi^2 + h^2}}, \tag{30}$$

$$\cos \varphi_2 = \frac{a + b - \xi}{\sqrt{(a + b - \xi)^2 + h^2}}. \tag{31}$$

Then the solution of the system of Eqs. (27)–(31) results in the desired relative position of the cable connector in the form

$$\xi^d = \frac{(c + h^d)\ddot{x}^d + a(\ddot{z}^d + g)}{\ddot{z}^d + g}, \tag{32}$$

which reduces exactly to Eq. (20) with the substitutions of expressions $x_{CC}^d = x^d - a + \xi^d$ and $z_{CC}^d = z^d + c + h^d$.

The above heuristic derivations demonstrates that due to the assumption of the horizontality of the swinging unit the complete planar model and the simplified double pendulum model result the same desired trajectory of the cable connector. Obviously the desired trajectory of the climber unit is also the same in both models.

5. Computed torque control method with backward Euler discretization

We apply the backward Euler discretization of the DAE system and the resulting set of equations are solved by the Newton–Raphson method for the desired actuator forces and uncontrolled coordinates and Lagrange multipliers.

We assume that the servo constraints result a $\mathbf{q}_c = \mathbf{q}_c^d$ for which the control input \mathbf{u} is bounded. Considering a PD controller with gain matrices \mathbf{K}_p and \mathbf{K}_D the control law can be formulated as:

$$\mathbf{M}\ddot{\mathbf{q}}^d + \Phi_q^T(\mathbf{q}^d)\lambda = \mathbf{Q}_g + \mathbf{H}(\mathbf{q}^d)\mathbf{u} - \mathbf{K}_p(\mathbf{q}^d - \mathbf{q}) - \mathbf{K}_D(\dot{\mathbf{q}}^d - \dot{\mathbf{q}}), \tag{33}$$

$$\boldsymbol{\varphi}(\mathbf{q}^d) = \mathbf{0}, \tag{34}$$

where \mathbf{q} is the measured and \mathbf{q}^d is the desired descriptor coordinate vector. The measured value of the coordinates appears only in the linear compensator.

Introducing $\mathbf{y}^d = \dot{\mathbf{q}}^d$ we derive the first order form of Eqs. (33) and (34). After the decomposition of the controlled and uncontrolled coordinates the control law can be written as:

$$\dot{\mathbf{q}}_c^d = \mathbf{y}_c^d, \tag{35}$$

$$\dot{\mathbf{q}}_u^d = \mathbf{y}_u^d, \tag{36}$$

$$\dot{\mathbf{y}}_c^d = \mathbf{S}_c^T \mathbf{M}^{-1} (-\Phi_q^T(\mathbf{q}^d)\lambda + \mathbf{Q}_g + \mathbf{H}(\mathbf{q}^d)\mathbf{u} - \mathbf{K}_p(\mathbf{q}^d - \mathbf{q}) - \mathbf{K}_D(\mathbf{y}^d - \dot{\mathbf{q}})), \tag{37}$$

$$\dot{\mathbf{y}}_u^d = \mathbf{S}_u^T \mathbf{M}^{-1} (-\Phi_q^T(\mathbf{q}^d)\lambda + \mathbf{Q}_g + \mathbf{H}(\mathbf{q}^d)\mathbf{u} - \mathbf{K}_p(\mathbf{q}^d - \mathbf{q}) - \mathbf{K}_D(\mathbf{y}^d - \dot{\mathbf{q}})), \tag{38}$$

$$\boldsymbol{\varphi}(\mathbf{q}^d) = \mathbf{0}. \tag{39}$$

Eq. (35) is identity thus we can leave it out of consideration. Eq. (36)–(39) can be discretized by the backward Euler method:

$$\frac{\mathbf{q}_{u,i+1}^d - \mathbf{q}_{u,i}^d}{h} = \mathbf{y}_{u,i+1}^d, \tag{40}$$

$$\frac{\mathbf{y}_{u,i+1}^d - \mathbf{y}_{u,i}^d}{h} = \mathbf{S}_u^T \mathbf{M}^{-1} (-\Phi_q^T(\mathbf{q}_{i+1}^d)\lambda_{i+1} + \mathbf{Q}_g + \mathbf{H}(\mathbf{q}_{i+1}^d)\mathbf{u}_{i+1} - \mathbf{K}_p(\mathbf{q}_{i+1}^d - \mathbf{q}_{i+1}) - \mathbf{K}_D(\mathbf{y}_{i+1}^d - \dot{\mathbf{q}}_{i+1})), \tag{41}$$

$$0 = -\dot{\mathbf{y}}_{c,i+1}^d + \mathbf{S}_c^T \mathbf{M}^{-1} (-\Phi_q^T(\mathbf{q}_{i+1}^d)\lambda_{i+1} + \mathbf{Q}_g + \mathbf{H}(\mathbf{q}_{i+1}^d)\mathbf{u}_{i+1} - \mathbf{K}_p(\mathbf{q}_{i+1}^d - \mathbf{q}_{i+1}) - \mathbf{K}_D(\mathbf{y}_{i+1}^d - \dot{\mathbf{q}}_{i+1})), \tag{42}$$

$$0 = \boldsymbol{\varphi}(\mathbf{q}_{i+1}^d). \tag{43}$$

Eqs. (40)–(43) constitute a system of $2n - l + m$ number of nonlinear equations for the $(i + 1)$ th value of the desired uncontrolled coordinates $\mathbf{q}_{u,i+1}^d$, their time derivatives $\mathbf{y}_{u,i+1}^d$, the control inputs \mathbf{u}_{i+1} and the Lagrange multipliers λ_{i+1} . It can be formulated as a function \mathbf{F}_{i+1} of the vector of unknowns $\mathbf{z} = [\mathbf{q}_{u,i+1}^d, \mathbf{y}_{u,i+1}^d + \mathbf{u}_{i+1} + \lambda_{i+1}]^T$ as follows:

$$\mathbf{F}_{i+1} = \begin{bmatrix} \mathbf{q}_{u,i+1}^d - \mathbf{q}_{u,i}^d - h\mathbf{y}_{u,i+1}^d \\ \mathbf{y}_{u,i+1}^d - \mathbf{y}_{u,i}^d - h\mathbf{S}_u^T \mathbf{M}^{-1} (-\Phi_q^T(\mathbf{q}_{i+1}^d)\lambda_{i+1} + \mathbf{Q}_g + \mathbf{H}(\mathbf{q}_{i+1}^d)\mathbf{u}_{i+1} - \mathbf{K}_p(\mathbf{q}_{i+1}^d - \mathbf{q}_{i+1}) - \mathbf{K}_D(\mathbf{y}_{i+1}^d - \dot{\mathbf{q}}_{i+1})) \\ \dot{\mathbf{y}}_{c,i+1}^d - \mathbf{S}_c^T \mathbf{M}^{-1} (-\Phi_q^T(\mathbf{q}_{i+1}^d)\lambda_{i+1} + \mathbf{Q}_g + \mathbf{H}(\mathbf{q}_{i+1}^d)\mathbf{u}_{i+1} - \mathbf{K}_p(\mathbf{q}_{i+1}^d - \mathbf{q}_{i+1}) - \mathbf{K}_D(\mathbf{y}_{i+1}^d - \dot{\mathbf{q}}_{i+1})) \\ \boldsymbol{\varphi}(\mathbf{q}_{i+1}^d) \end{bmatrix}. \tag{44}$$

The system of nonlinear equations is solved by Newton–Raphson method in the form $\mathbf{J}_{i+1}(\mathbf{z}_{i+1} - \mathbf{z}_i) = -\mathbf{F}_{i+1}$. The Jacobian is the following:

$$\mathbf{J}_{n+1} = \begin{bmatrix} \mathbf{I} & -h\mathbf{I} & \mathbf{0} & \mathbf{0} \\ h\mathbf{S}_u^T \mathbf{M}^{-1} \left(\frac{\partial(\Phi_q^T \lambda - \mathbf{H}\mathbf{u})}{\partial \mathbf{q}_u^d} + \mathbf{K}_p \mathbf{S}_u \right) & \mathbf{I} + h\mathbf{S}_u^T \mathbf{M}^{-1} \mathbf{K}_D \mathbf{S}_u & -h\mathbf{S}_u^T \mathbf{M}^{-1} \mathbf{H} & h\mathbf{S}_u^T \mathbf{M}^{-1} \Phi_q^T \\ \mathbf{S}_c^T \mathbf{M}^{-1} \left(\frac{\partial(\Phi_q^T \lambda - \mathbf{H}\mathbf{u})}{\partial \mathbf{q}_u^d} + \mathbf{K}_p \mathbf{S}_u \right) & \mathbf{S}_c^T \mathbf{M}^{-1} \mathbf{K}_D \mathbf{S}_u & -\mathbf{S}_c^T \mathbf{M}^{-1} \mathbf{H} & \mathbf{S}_c^T \mathbf{M}^{-1} \Phi_q^T \\ \Phi_q \mathbf{S}_u & \mathbf{0} & \mathbf{0} & \mathbf{0} \end{bmatrix}. \tag{45}$$

In some cases the Jacobian matrix may be ill-conditioned, but the problem can be handled by singular value decomposition where we leave out the relatively small elements.

6. Simulations and comparison with analytical results

The planar ACROBOTER model is examined with the present computed torque method based on the backward Euler discretization of the DAE system. The mechanical model can be seen in Fig. 4. The equations of motion is constructed as explained in [3].

The climber unit is modeled by a linear drive and its position is denoted by the coordinate x_1 . The cable connector is modeled by a point mass with mass m_{CC} and denoted by \mathbf{P}_2 in Fig. 4. The swinging unit is modeled by a rigid body with full mass m_{SU} and the descriptor coordinates is the outlet points of the secondary cables \mathbf{P}_3 and \mathbf{P}_4 respectively. The center of gravity of the swinging unit is denoted by \mathbf{CG} and ρ_{CG} points into its position in the body frame. Summarizing, the system is described by the redundant set of descriptor coordinates.

$$\mathbf{q} = [x_1 \ x_2 \ z_2 \ x_3 \ z_3 \ x_4 \ z_4]^T. \tag{46}$$

The position of the linear drive is controlled by force F_L the control forces act on cable L_1 L_2 and L_3 are F_1 F_2 and F_3 , respectively. Thus the control input can be written as:

$$\mathbf{u} = [F_L \ F_1 \ F_2 \ F_3]^T. \tag{47}$$

The mass of the swinging unit is $m_{SU} = 5$ kg and the cable connector is modeled by a point mass $m_{CC} = 0.5$ kg. The center of gravity is positioned in the midpoint of the L_{34} line. The distance of the cable outlet points \mathbf{P}_3 and \mathbf{P}_4 is fixed, so the geometric constraint vector is the following:

$$\boldsymbol{\varphi}(\mathbf{q}) = [(x_4 - x_3)^2 + (z_3 - z_4)^2 - L_{34}^2]. \tag{48}$$

A desired trajectory is defined for the midpoint of the L_{34} distance. According to Eq. (9) the servo constraint vector $\boldsymbol{\varphi}_s(\mathbf{q}, \mathbf{p}(t)) = \mathbf{h}(\mathbf{q}) - \mathbf{p}(t)$ is written with:

$$\mathbf{h}(\mathbf{q}) = \left[\frac{1}{2}(x_3 + x_4) \quad \frac{1}{2}(z_3 + z_4) \quad z_2 - \frac{1}{2}(z_3 + z_4) \quad z_3 - z_4 \right]^T, \tag{49}$$

$$\mathbf{p}(t) = [x^d \ z^d \ h_{CC}^d \ 0]^T, \tag{50}$$

from which we can see that the servo constraint and the geometric constraint together can be solved for the controlled coordinate $z_2 = z^d + h_{CC}^d$, $x_3 = x^d - \frac{1}{2}L_{34}$, $z_3 = z^d$, $z_4 = z^d$ and can be substituted into the control law (33), and (34).

The desired uncontrolled coordinate values x_1 , x_2 and x_4 , the Lagrange multiplier λ_1 and the desired forces F_L , F_1 , F_2 and F_3 are calculated by the computed torque control algorithm. The unknowns are scaled in order to obtain better conditioned system. The parallel simulation of the controlled dynamical system must be done at the same time because the linear compensator calculates a position and a velocity error $\mathbf{q}^d - \mathbf{q}$ and $\dot{\mathbf{q}}^d - \dot{\mathbf{q}}$. The simulation was accomplished with the Baumgarte stabilization of the equation of motion [3], which can be written as follows if the geometric constraints do not depend on time explicitly:

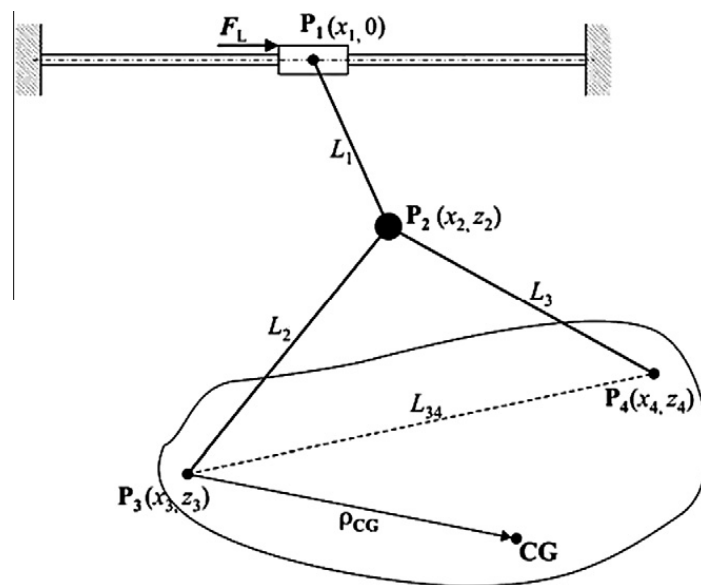


Fig. 4. The ACROBOTER model for numerical simulation.

$$\begin{bmatrix} \mathbf{M} & \Phi_q^T \\ \Phi_q & \mathbf{0} \end{bmatrix} \begin{bmatrix} \ddot{\mathbf{q}} \\ \lambda \end{bmatrix} = \begin{bmatrix} \mathbf{Q} \\ -\dot{\Phi}_q \dot{\mathbf{q}} - 2\alpha \Phi_q \dot{\mathbf{q}} - \beta^2 \boldsymbol{\varphi} \end{bmatrix}. \quad (51)$$

The gain matrices of the linear compensator are presently given as $\mathbf{K}_p = P\mathbf{H}_0\tilde{\mathbf{K}}$ and $\mathbf{K}_v = D\mathbf{H}_0\tilde{\mathbf{K}}$ with $P = 0.25 \text{ N/m}$, $D = 0.02 \text{ Ns/m}$ and

$$\tilde{\mathbf{K}} = \begin{bmatrix} 120 & -30 & 0 & 5 & 0 & 5 & 0 \\ 0 & 0 & 20 & 0 & 0 & 0 & 0 \\ 0 & 0 & 0 & 0 & 10 & 0 & 0 \\ 0 & 0 & 0 & 0 & 0 & 0 & 10 \end{bmatrix}. \quad (52)$$

Matrix $\tilde{\mathbf{K}}$ is tuned by trial and error method and \mathbf{H}_0 is the input matrix evaluated in a characteristic equilibrium configuration of the robot: $x_1 = 0 \text{ m}$, $x_2 = 0 \text{ m}$, $z_2 = -1 \text{ m}$, $x_3 = -\frac{1}{2}L_{34}$, $z_3 = -1.5 \text{ m}$, $x_4 = \frac{1}{2}L_{34}$ and $z_4 = -1.5 \text{ m}$.

In order to avoid the unbounded values occurring in the forward calculated control forces, the desired trajectories are given by C^∞ continuous analytical functions. The horizontal x^d and vertical position z^d of the swinging unit and the desired elevation h_{cc}^d of the cable connector above the swinging unit are prescribed by

$$\begin{aligned} x^d &= 0.25[\text{m}] \frac{2}{\pi} \arctan(2.5[1/\text{s}](t - 6[\text{s}])), \\ z^d &= -1.5[\text{m}] + 0.02[\text{m/s}]t, \\ h_{cc}^d &= 0.5[\text{m}]. \end{aligned}$$

The numerical simulations are accomplished with $dt = 0.01 \text{ s}$ time step, which requires that the controller must compute the desired control inputs in each 10 ms period. The tests showed that the on-board PC of the ACROBOTER prototype is capable of this challenge. Fig. 5 shows the results of the numerical simulation.

The desired value of the uncontrolled coordinate x_1 is calculated in closed form by the single and the double pendulum model, and x_1 is also calculated numerically. Fig. 5a shows that the result gained from the numerical simulation is closer to the result of the single pendulum model than the result of the double pendulum model. The experimental results (see Section 7) also showed that the application of the single pendulum model gives adequate results.

The sent out control force signals can be seen in Fig. 5b. F_1 is the main cable force F_2 and F_3 are the secondary cable forces. F_L is the force that is provided by the linear drive. After the initial perturbations the oscillations of the force signals are suppressed. The high acceleration of the swinging unit at $t = 6 \text{ s}$ also causes oscillations, especially in the F_L signal. The nominal value of the Lagrange multiplier λ_1 is also calculated by the control algorithm and depicted in Fig. 5c. The geometric constraint violation was under 10^{-10} m during the simulation.

The dashed curves show the desired path and the continuous curves show the simulated path of the points P_2 , P_3 and P_4 in Fig. 5d.

Fig. 5e shows the desired and the simulated horizontal position of the midpoint of the swinging unit. The desired value is given in $\mathbf{p}(t)$ and the simulated value is given by $\mathbf{h}(\mathbf{q})$. The error between the desired and the simulated value is depicted in Fig. 5f. In the initial configuration the horizontal position of the swinging unit has an error of 1 cm. As Fig. 5f shows, this error is decreased by the linear compensator.

The desired and simulated vertical position of the swinging unit and the error are shown in Fig. 5g and Fig. 5h. The initial error in the horizontal position causes oscillating error in the vertical position, but the compensation is significantly faster, because the cable winding actuators can act on the vertical position directly, while there is no direct actuation on the vertical position of the swinging unit and the cable connector.

The desired and the simulated elevation of the cable connector above the swinging unit is shown in Fig. 5i. The simulated tilt is shown in Fig. 5j, while the desired tilt is zero.

To summarize, the diagrams show that the computed torque control method with backward Euler discretization gives feasible control inputs, suppresses the error of the controlled coordinates, and the results are in strong connection with the analytical results.

7. Experimental results

Simulation and experimental results corresponding to the single pendulum model of ACROBOTER are presented in (Fig. 6). The required path of the robot (center of gravity of the swinging unit) was set to a slanted rectangle with 300 mm by 400 mm projected size onto the horizontal plane and with 130 mm elevation in the z direction. These dimensions correspond to maximum workspace of the prototype experimental setup, in which the climber unit and the winding actuator of the main suspending cable were emulated by a Hirata MB-H230/ MB-H180 3D Cartesian robot (see right in Fig. 1.). The single pendulum model is characterized by the estimated cable length of 820 mm and the weight 2.8 kg of the swinging unit, while the elevation of the cable connector with respect to the swinging unit was set to 500 mm.

The desired trajectories were calculated by using 6th order polynomial approximation of the required rectangular path. The top left panel in Fig. 3 presents one segment of this trajectory in the x direction, where the crosses denotes the data used

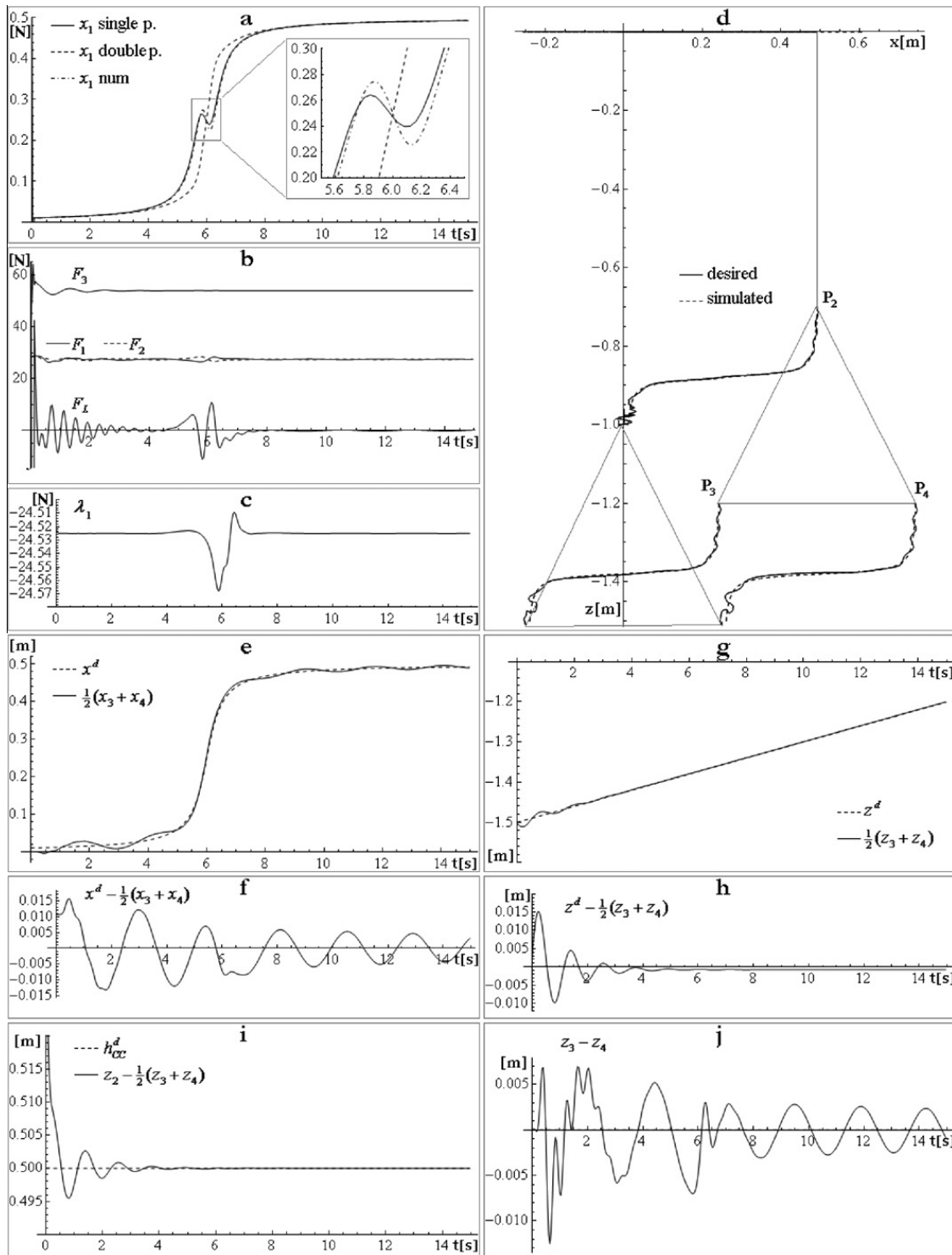


Fig. 5. The results of the numerical simulation.

for fitting the polynomial. The bottom left panel summarizes the results of the numerical simulations applied for the same desired trajectory segment. It shows that the calculated trajectories of the climber unit are close to each other in case of both the single and double pendulum models. During experiments the HIRATA robot were commanded to move along the simulated climber unit trajectories providing an open loop continuous path control for realizing the desired motion of the swinging unit. In the right panels of Fig. 5, the experimental results show that even the applied open loop controller can provide tolerable errors, since the maximum deviation (abs error) from the desired path remained below 60 mm that may be compensated by the ducted fans of the swinging unit.

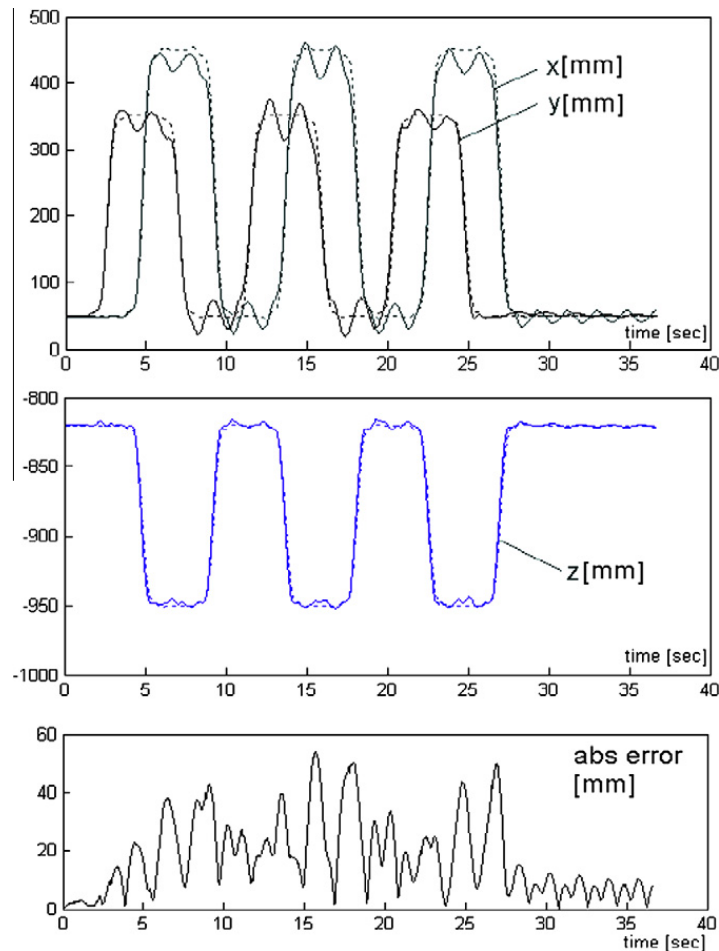


Fig. 6. Experimental results based on the single pendulum model.

8. Conclusion

By using single and double pendulum based dynamical models, the inverse dynamical problem of the under-actuated and redundant service robot platform ACROBOTER is solved in closed form. The applicability of these concepts is demonstrated by numerical simulation and experiments. Within the limitations of reasonable/practical restrictions the presented results can be generalized for a class of ceiling based service robots including the complex 3D model of the ACROBOTER system.

A formalism was proposed for the computed torque control of under-actuated and furthermore natural coordinate based dynamical systems. The numerical simulations showed the applicability of the algorithm. The simulation also showed that the method gives the same results as the analytical solution of the inverse dynamic problem.

Our studies indicated that in case of more complex and larger systems the Jacobian matrix may be ill-conditioned. The examination of this problem is a future work.

The feasibility of the present control approach is planned to be tested in the framework of the ACROBOTER project.

Patents pending

Application No.: HU-P0900466. Application date: July 28, 2009. Title: "Payload suspension system". Application No.: HU-P0900467. Application date: July 28, 2009. Title: "Suspended payload platform thrust by fluid mass flow generators".

Acknowledgements

This work was supported in part by the Hungarian National Science Foundation under Grant No. OTKA K068910, the ACROBOTER (IST-2006-045530) project, the Hungarian Academy of Sciences under Grant No. MTA-NSF/103, and by the HAS-BME Research Group on Dynamics of Machines and Vehicles.

References

- [1] Goldstein H. *Classical Mechanics*. second ed. Reading, MA: Addison-Wesley; 1980. 672 pages.
- [2] Wen JT-Y. *Control of Nonholonomic Systems*. In: Levine WS, editor. *Control Handbook*. Boca Raton, FL: CRC and IEEE; 1996. p. 1359–68.
- [3] de Jalón JG, Bayo E. *Kinematic and Dynamic Simulation of Multibody Systems: The Real-Time Challenge*. Springer-Verlag; 1994.
- [5] Henry RJ, Masoud ZN, Nayfeh AH, Mook DT. Cargo pendulation reduction on ship-mounted cranes via Boom-Lu[®] angle actuation. *Journal of Vibration and Control* 2001;7(8):1253–64.
- [6] Blajer W, Kołodziejczyk K. Modeling of underactuated mechanical systems in partly specified motion. *Journal of Theoretical and Applied Mechanics* 2008;46(2):383–94.
- [7] Stépán G, Toth A, Kovacs LL, Bolmsjö G, Nikoleris G, Surdilovic D, Conrad A, Gasteratos A, Kyriakoulis N, Chrysostomou D, Kouskouridas R, Canou J, Smith T, Harwin W, Loureiro R, Lopez R, Moreno M. A ceiling based crawling, hoisting and swinging service robot platform. In: *Proceedings of beyond gray droids: domestic robot design for the 21st century workshop at HCI 2009*, September 1–5, Cambridge, UK; 2009. Available from: <http://www.cl.cam.ac.uk/conference/drd09/papers/toth.pdf>.
- [8] Kövecses J, Piedoboeuf J-C, Lange C. Dynamic modeling and simulation of constrained robotic systems. *IEEE/ASME Transactions on Mechatronics* 2003;8(2):165–77.
- [9] Sato T, Fukui R, Mofushita H, Mori T. Construction of Ceiling Adsorbed Mobile Robots Platform Utilizing Permanent Magnet Inductive Traction Method, in *Proceedings of 2004 IEEEiRSJ International Conference on Intelligent Robots and Systems*, September 28–October 2, 2004, Sendai, Japan, 552–558.
- [10] McKerrow PJ, and Ratner D. The design of a tethered aerial robot, in *Proceedings of International Conference on Robotics and Automation*, Rome, Italy, 10–14 April 2007, 335–360.
- [11] Blajer W, Dziewiecki K, Kołodziejczyk K, Mazur Z. Inverse Dynamics of a Two-Degree Freedom Underactuated System: Analysis and Experiment. 10th Conference on Dynam Systems - Theory and Applications DSTA-2009, December 7–10 Łódź, Poland.
- [12] Zelei A, Kovács LL, Stépán G. Computed Torque Control Method for Under-Act Manipulator. In: *Proceedings of the ASME 2009 International Design Engineering Technical Conferences & Computers and Information in Engineering Conference*, San Diego, California USA, 2009. Paper DETC2009-86409.
- [13] Omar, H.M., Nayfeh, A.H.: *Control of Gantry and Tower Cranes*. Virginia Polytec Institute and State University, 2003.
- [14] Lammerts, I.M.M. *Adaptive Computed Reference Computed Torque Control*. Eindh University of Technology, 1993.